The double *par* locus of virulence factor pB171: DNA segregation is correlated with oscillation of ParA

Gitte Ebersbach and Kenn Gerdes*

Department of Biochemistry and Molecular Biology, University of Southern Denmark, Campusvej 55, DK-5230 Odense M, Denmark

Communicated by Nancy Kleckner, Harvard University, Cambridge, MA, October 25, 2001 (received for review May 25, 2001)

Prokaryotic plasmids and chromosomes encode partitioning (*par*) loci that segregate DNA to daughter cells before cell division. Recent database analyses showed that almost all known *par* loci encode an ATPase and a DNA-binding protein, and one or more cis-acting regions where the proteins act. All *par*-encoded ATPases belong to one of two protein superfamilies, Walker-type and actin-like ATPases. This property was recently used to divide *par* loci into Types I and II loci. We show here that the *Escherichia coli* virulence factor pB171 encodes a double *par* locus that consists of one Type I and one Type II locus. Separately, each locus stabilized a test-plasmid efficiently. Together, the two loci mediated even more efficient plasmid stabilization. The *par* loci have a unique genetic organization in that they share a common central region at which the two different DNA-binding proteins probably act. Interestingly, a fusion protein consisting of the Walker-type ParA ATPase and Gfp was functional and oscillated in nucleoid regions on a time scale of minutes. ParA-green fluorescent protein (Gfp) oscillation depended on both ParB and *parC* but was independent of *minCDE*. Point mutations in the Walker A box motif simultaneously abolished plasmid stabilization and ParA-Gfp oscillation. These observations raise the possibility that ParA oscillation is prerequisite for active plasmid segregation.

ATPase | Gfp | partitioning | plasmid segregation

Prokaryotic plasmids and chromosomes specify functions that ensure segregation of DNA molecules before cell division (1–4). Plasmid- and chromosome-encoded partitioning (*par*) loci encode two trans-acting proteins, usually called ParA and ParB, and one or more cis-acting DNA regions where the proteins act (denoted *parS* or *parC*). ParB proteins interact with the cis-acting sites and with ParA proteins. In all cases investigated, ParA proteins possess ATPase activity (5–9). Although both plasmid-encoded and, more recently, also chromosome-encoded *par* loci have been analyzed thoroughly, the molecular mechanisms behind active DNA movement in prokaryotes have remained elusive.

The ParA proteins belong to two different superfamilies of ATPases, and recently this property was used to divide plasmid-encoded partitioning loci into two types (4). Type I loci encode ATPases containing the so-called deviant Walker-type motif also found in MinD proteins (10). All chromosome- and almost all plasmid-encoded partitioning loci encode this type of ATPase, and more than 100 ParA homologous proteins can now be retrieved from the databases (4, 11, 12). The function of the ATPases in plasmid segregation is not known. However, the *par* loci of P1 and F position plasmid copies subcellularly in a nonrandom fashion (13–15), and the positioning depends on the Walker-type ATPases (ParA and SopA). In most cells, *par*-encoding plasmids were located either at mid- or quarter-cell positions. The quarter-cell position is the future midcell in the next cell generation. Thus, during progression of the cell cycle, the ATPases of F and P1 seem to be required for relocalization of plasmids from mid- to quarter-cell positions.

Type II partitioning loci encode actin-like ATPases (9, 16). The model locus *par* of plasmid R1 encodes the actin-like ParM ATPase and the DNA-binding ParR protein. The cis-acting *parC* region is located upstream of the *parMR* operon and contains 10 direct repeats to which ParR binds (17–20). ParM interacts with ParR *in vitro* when ParR is bound to *parC*-DNA (9, 20). In the case of *par* of R1, plasmid copies also localize nonrandomly. Thus, *par*-encoding plasmid copies were positioned either at midcell or close to the cell poles (21). This nonrandom subcellular positioning depended on ParM. The DNA-binding protein ParR mediates pairing of plasmid molecules at *parC in vitro* (20). This information, combined with the symmetrical pattern of plasmid localization *in vivo*, suggests that plasmid molecules are replicated at midcell, become paired via ParR/*parC* (21), and then move in opposite directions toward the cell poles.

The specific DNA regions at which ParB/ParR proteins bind also exert partition-related incompatibility. For example, if *parC* of plasmid R1 is present on a high-copy-number plasmid in a strain also carrying a plasmid stabilized by *par* of R1, then the R1 plasmid becomes unstable (17, 19). The mechanism of this interference phenomenon is not known. The high-copy plasmid carrying *parC* could exert incompatibility directly; for example, heterologous pairing with the R1 plasmid might interfere with proper sister plasmid segregation. Alternatively, titration of ParR by *parC* might interfere with proper *par* function.

Here we show that the *Escherichia coli* virulence plasmid pB171 encodes two different *par* loci that both mediate plasmid stabilization. Genetic experiments indicate that the two *par* loci share a common central cis-acting region. Interestingly, a ParA-green fluorescent protein (Gfp) fusion protein localized to nucleoid regions and oscillated within the nucleoid regions. Oscillation depended on the presence of the other components of the *par* locus (ParB and *parC*). These results expand the functions for oscillating cell cycle proteins to include also DNA segregation.

Materials and Methods

Bacterial Strains. *E. coli* strain MC1000 [Δ(*ara-leu*) Δ*lac rpsL150*] (22) and KG22 (C600 *lacI*^{q} *lacZ*Δ*M15*) were used in plasmid stability assays. M2141 (*minB lac pro rpsL*) is a minicell-producing strain (23). Resistance factor pB171 of enteropathogenic *E. coli* was obtained from T. Tobe (24), plasmid pMH82 was from A. K. Nielsen (25), and M. Mikkelsen constructed the pBR322-based expression-vector pMG25.

Plasmids Used and Constructed. Plasmids used to assay for activity of *par1*, *par2*, or *par12* were constructed by inserting the relevant PCR fragments of pB171 into the miniR1 *lacZYA* test vectors pRBJ200 (*bla*) or pMH82 (*aphA*). Plasmids derived from pMH82 carry the suffix K (for kanamycin resistance). The following oligonucleotides were used as PCR primers: pGE103, pB171–1 and pB171–9; pGE2 and pGE2K; pB171–4 and pB171–2; pGE201, pB171–4 and pB171–8; and pGE3, pB171–1, and pB171–2. Plasmid pGE202K carries an in-frame deletion of 71 codons within *parA*, created by

Abbreviations: LF, loss frequencies per cell per generation; DAPI, 4′,6-diamidino-2-phenylindole; IPTG, isopropyl β-D-thiogalactoside; Gfp, green fluorescent protein.

*To whom reprint requests should be addressed. E-mail: kgerdes@bmb.sdu.dk.

The publication costs of this article were defrayed in part by page charge payment. This article must therefore be hereby marked "*advertisement*" in accordance with 18 U.S.C. §1734 solely to indicate this fact.

www.pnas.org/cgi/doi/10.1073/pnas.261569598

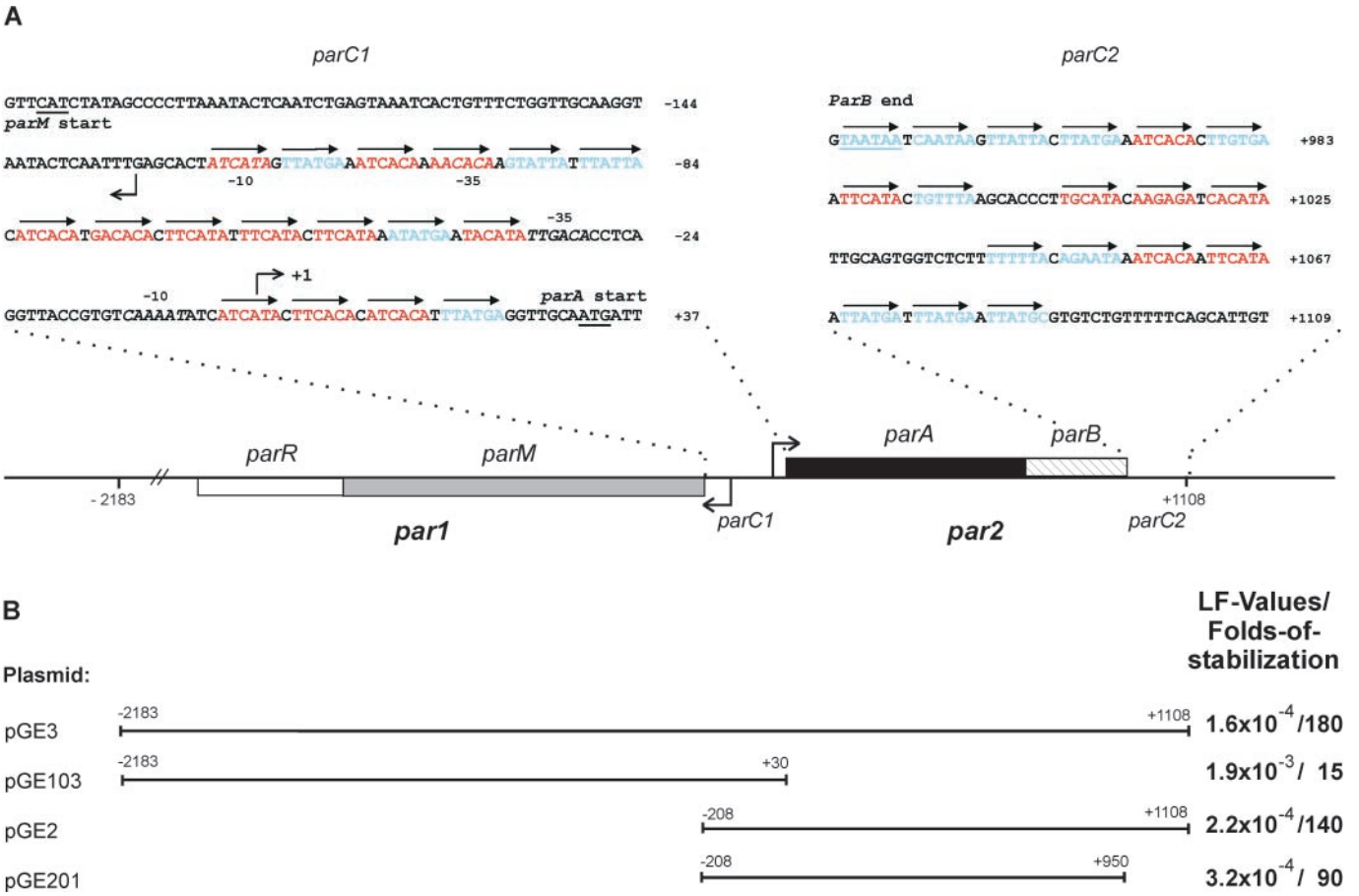

Fig. 1. Overview of the *par12* locus of pB171 (*A*) and of pB171-derived DNA fragments used in plasmid-stability tests (*B*). *A* shows the genetic organization of *par1* and *par2*, *parC1* and *parC2*. The gene encoding the actin-like ParM protein is shown as a gray box, *parR* as an open box, *parA* encoding the Walker-type ATPase as a black box, and *parB* is hatched. The DNA sequences of *parC1* and *parC2* are shown in blowups; arrows indicate direct repeats. Red, class I repeats; blue, class II repeats. Broken arrows pointing left and right indicate the transcription start points for the *par1* and *par2* operons, respectively. Numbering of base pairs according to the transcription start point of *par2* (denoted +1). *B* shows extensions of PCR-derived DNA fragments inserted into the R1 test vector pRBJ200 and their effect on plasmid stability given as LF values measured as described by Gerdes *et al.* (40). Folds of stabilization relative to pRBJ200 (LF = 10^{-2} per cell per generation) of the respective plasmids are also shown. LF values are averages of five independent experiments for all four plasmids. LF values and their standard deviations: pGE3: $(1.6 \pm 0.55) \times 10^{-4}$; pGE103: $(1.9 \pm 0.58) \times 10^{-3}$; pGE2: $(2.2 \pm 0.87) \times 10^{-4}$; pGE201: $(3.2 \pm 0.84) \times 10^{-4}$.

digestion of pGE2K with *Eco*RI followed by religation. Plasmids pGE303 and pGE304 were constructed by PCR amplification of, respectively, *parC1* and *parC2* and cloning of the resulting fragments into the *Pst*I-*Eco*RI sites (pGE303) or *Pst*I-*Aat*II sites (pGE304) of pBR322. The following primers were used for the PCR: pGE303, pB171–6, and pB171–9; and pGE304, pB171–10, and pB171–11. A *parC1*-containing PCR fragment was cloned between the *Eco*RI and *Bam*HI sites of pMH82, resulting in pGE313. Plasmid pGE220 was constructed by PCR amplification of *parA* from pB171 by using primers pB171–14 and pB171–15. The PCR product was cloned into vector pEGFP (CLONTECH). Subsequently, p*lac*::*parA*::*gfp* of pGE220 was inserted into the *Swa*I site of the following plasmids: pMH82 creating pGE230, pGE2K creating pGE233, pGE202K creating pGE236, and pGE313 creating pGE331. Plasmid pGE30K is pMH82 encoding LacZ′-Gfp. Plasmid pGE236G10V contains a single amino acid substitution within *parA* in *parA*::*gfp* of pGE236. Plasmid pGE236G10V was constructed by replacement of the *Psi*I-*Age*I fragment of *parA*::*gfp* within pGE236 with a fragment containing the appropriate point mutation introduced by PCR, by using the following oligonucleotides as primers: pB171–26 and pB171–28. Plasmid pGE236K14Q was constructed in a similar way by using primers pB171–27 and pB171–28. Plasmid pGE223 encodes the His-tagged ParB protein constructed by using primers pB171–20 and pB171–21 inserted into plasmid pMG25. Plasmid pGE223 carries *lacI* and expresses His-tagged ParB on addition of isopropyl β-D-thiogalactoside (IPTG) to growing cells. Sequences of primers used for PCR amplifications are available on request.

Microscopy. Strain KG22 harboring relevant plasmid was grown overnight at 30°C in A + B minimal medium (26) plus 0.2% glucose/1 μg/ml of thiamine/0.05% (or 0.01%) casamino acids. Cultures were diluted 50-fold, grown to $OD_{450} \approx 0.03$–0.04, and ParA-Gfp synthesis induced by IPTG. The generation time of the strains under these growth conditions was ≈75 min (or 130 min). Three to four hours after induction, a sample of cell culture was immobilized on microscope slides by using a thin film of 1% agarose. Living cells were observed as described previously (21).

Results

The Unusual Double *par* Operon of Plasmid pB171. By database searching, we found that *E. coli* virulence plasmid pB171 contains two adjacent divergently oriented partitioning loci belonging to the two different classes of known *par* loci (see Introduction). We denote the two *par* loci of pB171 *par1* and *par2*, respectively (Fig. 1). *par1* encodes two putative proteins, ParM (323 amino acids) and ParR (130 amino acids), which are homologous to ParM (actin-like) and ParR of plasmid R1, respectively. Similarly, *par2* encodes two

GENETICS

Table 1. Incompatibility exerted by *parC1* and *parC2*

Second plasmid	R1 test plasmid			
	pRBJ200 (*par*$^-$)	pGE103 (*par1*)	pGE2 (*par2*)	pGE3 (*par12*)
pBR322 (vector)	1.9×10^{-2} (≡1)	7.7×10^{-4} (≡1)	1.4×10^{-4} (≡1)	8.9×10^{-5} (≡1)
pGE303 (*parC1*)	2.1×10^{-2} (1)	3.9×10^{-3} (5)	1.9×10^{-2} (130)	9.2×10^{-3} (100)
pGE304 (*parC2*)	2.0×10^{-2} (1)	7.5×10^{-4} (1)	1.5×10^{-2} (110)	6.7×10^{-4} (8)

Numbers are LF values of the R1 test plasmids in the presence of the second plasmids pGE303 (*parC1*) or pGE304 (*parC2*) and are in all cases averages of three independent experiments. Numbers in parentheses are folds of destabilization (changes in LF values relative to the effect of pBR322) caused by the second plasmid (pBR322 derivatives). The effect of the pBR322 vector was set to 1. Cells of MC1000 were grown at 30°C in LB medium containing 10 μg/ml of tetracycline, thus selecting for the second plasmid (pBR322 derivatives). The plasmid vector used to construct the test plasmids was in all cases pRBJ200. Coordinates of the *parC* fragments are given in the text.

proteins, ParA (214 amino acids) and ParB (91 amino acids). The putative ParA protein belongs to the ParA/SopA family, all of which contain the deviant Walker-type ATP-binding motifs (10, 27). ParA of pB171 belongs to the Ib subgroup of partitioning proteins also including ParA of pTAR from *Agrobacterium tumefaciens* and ParF from *Salmonella newport* plasmid TP228 (4, 11).

The promoter regions of *par1* and *par2* are adjacent and divergently oriented (Fig. 1*A*). Putative −10 and −35 promoter elements were readily recognized, and promoter activities were confirmed by primer extension analysis (not shown). The transcription start site of the *par2* operon was mapped to the nucleotide located 31 bp upstream of the *parA* start codon. The major transcription start site of *par1* was located on the opposite strand, 67 bp upstream of the start codon of *parM*. Thus, the promoters of *par1* and *par2* are separated by only 131 bp (Fig. 1*A*). We inspected the double promoter region for the presence of direct repeats. We found two clusters of 6-bp repeats, one consisting of 13 and another of 4 repeats, the latter being located between the *par2* promoter and the start codon of *parA* (Fig. 1*A*). The repeats are in all cases separated by 1 bp. We denote the region containing the 17 repeats *parC1*. Likewise, the region downstream of *parB* contained 18 6-bp direct repeats organized into three clusters. Consequently, the 160-bp region downstream of *parB* was denoted *parC2* (Fig. 1*A*). The repeats in *parC1* and *parC2* are related and could be divided into two subclasses (Fig. 1*A*, colored bases), from which two consensus sequences were derived. Thus, class I repeats have the consensus sequence [AT][TA]CA[TC]A and class II repeats TTAT[GT]A (alternative bases in brackets). The two classes of repeats are randomly distributed in *parC1* and *parC2* but with a slight preponderance of class I repeats in *parC1* and class II repeats in *parC2* (Fig. 1*A*).

***par1* and *par2* Both Contribute to Plasmid Segregation.** DNA fragments containing *par1*, *par2*, or *par1* plus *par2* were PCR amplified, cloned into a test vector, and sequenced (Fig. 1*B*). The test vector used, pRBJ200, was a *par*$^-$ R1 plasmid characterized by a loss rate of approximately 0.01 per cell per generation. The stability phenotypes conferred by the cloned DNA fragments were accurately measured in long-term plasmid-stability assays (80 generations) by using *E. coli* strain MC1000 as the host strain (Fig. 1*B*). *par1* (in pGE103) stabilized the R1 vector 15-fold, implying that *par1* by itself constitutes an active partitioning locus (the absolute loss frequencies are given in Fig. 1*B*). *par2* (in pGE2) stabilized the R1 vector 140-fold, implying that *par2* also constitutes an active partitioning locus. *par1* plus *par2* (in pGE3) stabilized the test vector 180-fold, consistent with the notion that both *par* loci simultaneously contribute to stabilize their replicon.

The *par2* fragment contains both *parC1* and *parC2* (Fig. 1*A*). The downstream direct repeats (*parC2*) of pGE2 were deleted, resulting in pGE201. This plasmid yielded a 90-fold stabilization, implying that *parC2* significantly contributes to the stabilizing effect of *par2* (Fig. 1*B*).

***parC1* Exerts Incompatibility Toward *par1* and *par2*.** In all previous cases investigated, *par*-encoded direct repeats exert incompatibility. *parC1* (−192 to +30) was cloned into a high-copy-number replicon (pBR322), and the resulting plasmid (pGE303) was introduced into strains MC1000/pGE103 (*par1*), MC1000/pGE2 (*par2*), MC1000/pGE3 (*par12*) and into MC1000 containing the proper control vector plasmid (pRBJ200). Table 1 shows that the presence of *parC1* in high copy (pGE303) destabilized the *par1* plasmid 5-fold, the *par2* plasmid 130-fold, and the *par12* plasmid 100-fold. Thus the central *parC1* region destabilized plasmids carrying either *par1* or *par2*, or both. *parC1* destabilized *par2* more than it destabilized *par1*.

***parC2* Exerts Incompatibility Toward *par2* but Not Toward *par1*.** Plasmid pGE304, a pBR322 derivative carrying *parC2* (+920 to +1108), was analyzed in a similar way. Interestingly, pGE304 destabilized the *par2* plasmid (pGE2) 110-fold and was thus in this respect almost as efficient as *parC1* (Table 1). However, the *parC2*-carrying plasmid did not destabilize the *par1*-carrying plasmid pGE103 at all. The *par12*-carrying plasmid pGE3 was also destabilized significantly (8-fold) by *parC2* (Table 1). This result suggests that *parC2* is a component of *par2* but not of *par1*.

ParA-Gfp Is Functional. Introduction of an in-frame deletion of 71 codons in *parA* inactivated *par2*, showing that *parA* is essential (pGE202K in Table 2). The *parA* gene was then fused to a bright variant (*mut1*) of *gfp*. A DNA fragment encoding p*lac*::*parA*::*gfp* was inserted into the R1 plasmid carrying the deletion in *parA*, resulting in pGE236 (*par2* Δ*parA* p*lac*::*parA*::*gfp*). The stability of pGE236 was measured in KG22 (*lacI*^{q}) without the addition of IPTG. Importantly, the insertion of the p*lac*::*parA*::*gfp* fragment yielded a 75-fold increase in stability, indicating that ParA-Gfp is at least partially functional [for absolute loss frequencies per cell per generation (LF) values, compare pGE236 and pGE202K in Table 2]. Higher expression levels of ParA-Gfp did not increase stability of pGE236 (not shown).

The p*lac*::*parA*::*gfp* fragment was also inserted into an R1 plasmid encoding the entire *par2* locus (pGE2K), resulting in pGE233 (*par2* p*lac*::*parA*::*gfp*). Plasmid pGE233 was less stable than its parent plasmid pGE2K (*par2*), showing that the presence of *parA*::*gfp* interfered with *par2* activity (Table 2). However, pGE233 (*par2* p*lac*::*parA*::*gfp*) was 40-fold more stable than pGE230 carrying plac::*parA*::*gfp* without *par2*.

ParA-Gfp Oscillates. We examined the subcellular localization of ParA-Gfp in living cells by using fluorescence microscopy. In a little more than half of fluorescent KG22 cells harboring either pGE233 (*par2* p*lac*::*parA*::*gfp*) or pGE236 (*par2* Δ*parA*

Table 2. Correlation of plasmid stabilization and ParA-Gfp oscillation

Plasmid*	*par2* components†	LF values‡	Folds of stabilization	Oscillation of ParA-Gfp
pMH82	None	2.0×10^{-2}	1.0	No ParA-Gfp
pGE2K	*parC1 parA parB parC2*	1.3×10^{-4}	150	No ParA-Gfp
pGE202K	*parC1* Δ*parA parB parC2*	2.0×10^{-2}	1.0	No ParA-Gfp
pGE236	*parC1* Δ*parA parB parC2 parA*::*gfp*	2.7×10^{-4}	75	+
pGE236G10V	*parC1* Δ*parA parB parC2 parA(G10V)*::*gfp*	2.0×10^{-2}	1.0	−
pGE236K14Q	*parC1* Δ*parA parB parC2 parA(K14Q)*::*gfp*	3.2×10^{-2}	0.6	−
pGE233	*parC1 parA parB parC2 parA*::*gfp*	5.0×10^{-4}	40	+
pGE230	*parA*::*gfp*	1.7×10^{-2}	1.2	−

*All plasmids were derived from pMH82, a *par*$^-$ R1 test vector.
†Δ indicates a 213-bp in-frame deletion in *parA*.
‡LF values are defined in the legend to Fig. 1. Plasmid-containing cells of strain KG22 (*lacI*^{q}) were grown in LB medium at 30°C without IPTG. Culture dilutions were plated on LA plates containing X-gal (40 μg/ml) to determine the frequency of plasmid-containing cells. Numbers are in all cases averages of at least three independent experiments.

p*lac*::*parA*::*gfp*), the signal was positioned asymmetrically in one-half of the cell only, appearing either as a distinct focus or as an elongated drop-shaped structure (Fig. 2*A*). The rest of the fluorescent cells showed a weaker and more diffuse fluorescence pattern. Thirty percent of all cells harboring pGE233 or pGE236 showed no fluorescence. Interestingly, time-lapse experiments revealed that ParA-Gfp oscillated from one end of the cell to the other on a time scale of minutes (compare Fig. 2*A Left* and *Right*).

Next, we followed individual cells of KG22 carrying pGE233 (*par2* p*lac*::*parA*::*gfp*) in time-lapse experiments. Fig. 2*B* shows a typical sequence of events starting with a ParA-Gfp focus located near one end of a cell. During the following 6–10 min, the focus disintegrated, and the fluorescent signal moved to the opposite end where a new bright focus was assembled. The foci very rarely reached the ultimate cell poles. Oscillation time depended on the length of the cell, with the oscillation time being longest in the longer cells. This cell-length dependency was especially prominent in the long cells of the minicell-producing strain (Fig. 2*J*; see below). In some cells, the focus repeated the oscillation cycle almost immediately, whereas in others it seemed to be at rest for several minutes before it resumed moving. In a minor portion of the cells, the newly formed foci were stationary, at least for as long as fading of the fluorescent signal allowed additional images to be acquired.

We also determined oscillation of ParA-Gfp in a strain lacking any wild-type ParA protein. Fig. 2*C* shows that ParA-Gfp from pGE236 (*par2* Δ*parA* p*lac*::*parA*::*gfp*) oscillated. Thus, ParA-Gfp exhibited dynamic behavior even without the presence of native ParA. The oscillation frequencies were similar in the two different genetic backgrounds (Fig. 2 *B* and *C*).

ParA-Gfp Oscillation Depends on ParB and *parC*. To determine whether oscillation depended on other genetic determinants of the *par2* locus, we examined ParA-Gfp in other R1 derivatives. First, ParA-Gfp was examined in cells harboring pGE230, a R1 derivative containing *plac*::*parA*::*gfp* but neither *parB* nor *parC* (Table 2). In these cells, ParA-Gfp fluorescence did not oscillate and was evenly distributed (Fig. 2*G*). Thus, formation and oscillation of ParA-Gfp foci required the presence of ParB and/or *parC*.

To generate cells producing ParA-Gfp and ParB, plasmid pGE223 (p*lac*::*his6*::*parB*), which expresses a functional His-tagged version of ParB protein, was introduced into KG22 carrying pGE230 (p*lac*::*parA*::*gfp*). ParA-Gfp produced by the resulting strain, KG22/pGE230 (p*lac*::*parA*::*gfp*)/pGE223 (p*lac*::*his6*::*parB*), did not oscillate (Fig. 2*E*). Thus, ParA-Gfp did not oscillate in the presence of ParB without *parC*.

Next, cells expressing ParA-Gfp in the presence of *parC1*, but without *parB*, were examined. ParA-Gfp produced by KG22/pGE331 (*parC1 plac*::*parA*::*gfp*) did not oscillate (Fig. 2*D*).

Finally, plasmid pGE223 (p*lac*::*his6*::*parB*) was introduced into cells carrying pGE331 (*parC1 plac*::*parA*::*gfp*). In this case, oscillation was regained (Fig. 2*F*). Together, these results show that ParA-Gfp oscillation requires the presence of ParB and at least *parC1*. Moreover, ParA-Gfp oscillated even though ParB was donated in trans.

Oscillation of ParA-Gfp Does Not Depend on *minCDE*. ParA-Gfp in the minicell-producing strain M2141 (*minB*) carrying pGE236 (*par2* Δ*parA* p*lac*::*parA*::*gfp*) oscillated (Fig. 2*J*). Thus, ParA-Gfp oscillation was independent of the *minCDE* system. Many cells of the minicell-producing strain appeared elongated. In such cells, ParA-Gfp cycling time was considerably increased, typically in the order of 30 min at the conditions used here (Fig. 2*J*).

Walker A Box Mutations in ParA-Gfp Simultaneously Abolish Oscillation and Plasmid Stabilization. Single amino acid changes were introduced into the conserved ATP-binding domain (Walker A box motif) of ParA-Gfp. Glycine at position 10 was changed to valine and lysine at position 14 to glutamine. Lysine 14 (or its equivalent) is nearly invariable in all Walker A boxes (10, 27) and interacts with the α- and β-phosphates of the bound nucleotide (28, 29). Mutations in the conserved lysine typically disrupt nucleotide binding (30). Microscopy revealed that cells of KG22 carrying plasmids pGE236G10V [*par2* Δ*parA* p*lac*::*parA*(G10V)::*gfp*] or pGE236K14Q no longer showed asymmetric distribution of the ParA-Gfp fusion proteins, and the proteins did not oscillate (Fig. 2 *H* and *I*). Plasmid stability assays revealed that pGE236G10V and pGE236K14Q were unstably inherited (Table 2). Thus, mutational change of conserved amino acids within the Walker A box of ParA simultaneously abolished the oscillating behavior of the fusion protein and its ability to mediate plasmid stabilization.

ParA-Gfp Colocalizes with Nucleoids. During oscillation, the ParA-Gfp signal rarely reached the ultimate cell poles and was often asymmetrically distributed (Fig. 2 *A* and *C*). 4′,6-diamidino-2-phenylindole (DAPI) staining of cells harboring pGE236 (*par2* Δ*parA* p*lac*::*parA*::*gfp*) indicated that the Gfp signal coincided with nucleoid regions (Fig. 2*K*). The DAPI-stained nucleoid DNA appeared stationary, showing that ParA-Gfp, not the DNA, moved. To substantiate the presumed nucleoid localization of ParA-Gfp, we also investigated filamentous multinucleate cells containing pGE230 (p*lac*::*parA*:.*gfp*) obtained by treatment with cephalexin and chloramphenicol (the latter condenses the nucleoids). In such cells, DAPI staining showed that nucleoids were evenly distributed along the cell filaments (Fig. 2*L*). The ParA-Gfp signal exhibited a very similar distribution (Fig. 2*L*′),

GENETICS

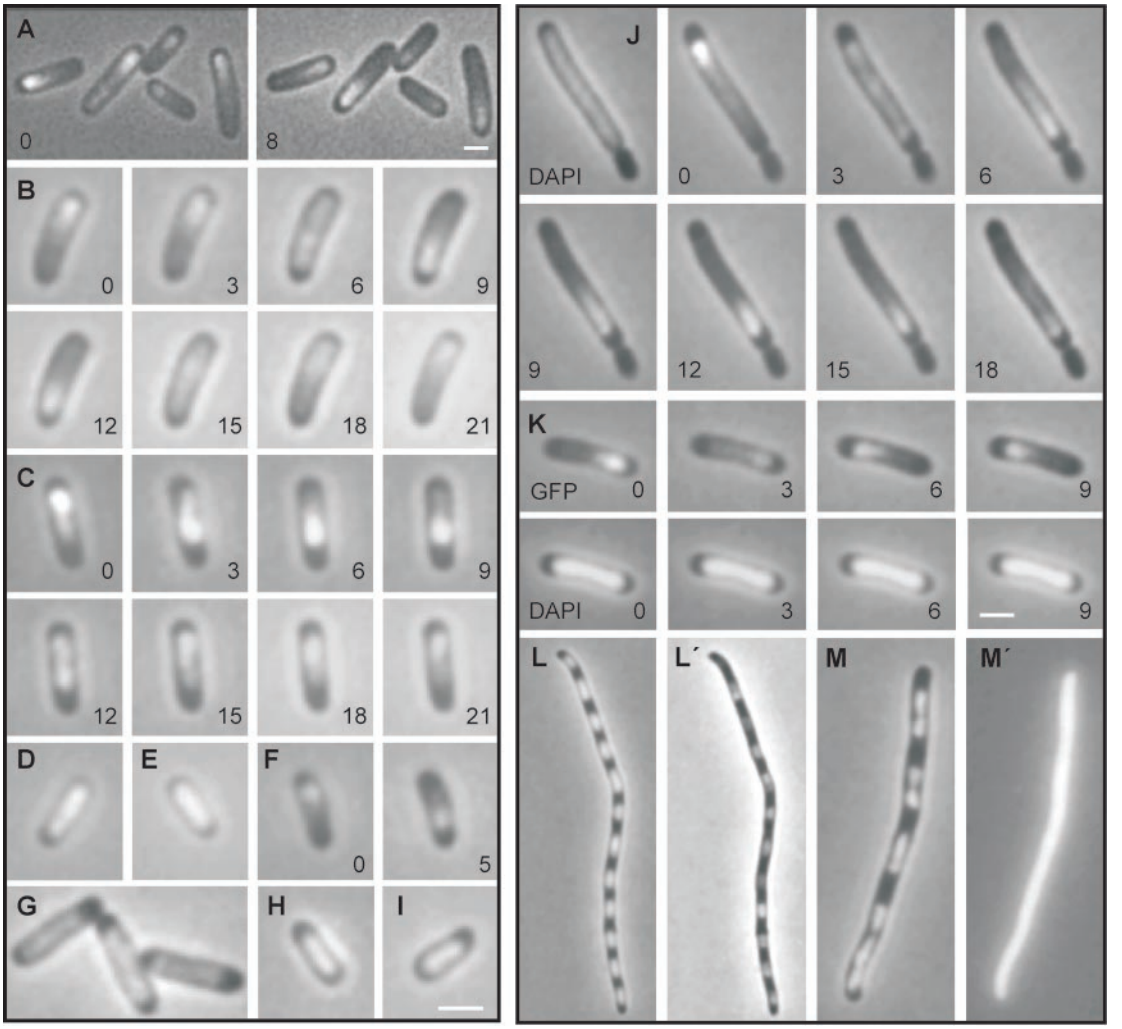

Fig. 2. Dynamic properties of functional ParA-Gfp in live cells. Combined phase contrast and fluorescent microscopy of ParA-Gfp-containing KG22 cells grown as described in *Materials and Methods* in the presence of 100 μM IPTG except in *E* and *F* (10 μM IPTG). Numbers are minutes in time-lapse experiments. (*A*) ParA-Gfp from pGE233 (*par2* p*lac*::*parA*::*gfp*). *Left* and *Right* show the same cells; (*B*) a complete cycle of ParA-Gfp from pGE233 (*par2* p*lac*::*parA*::*gfp*); (*C*) a complete oscillation cycle of ParA-Gfp from pGE236 (*par2* Δ*parA* p*lac*::*parA*::*gfp*); (*D*) ParA-Gfp from pGE331 (*parC1* p*lac*::*parA*::*gfp*); (*E*) ParA-Gfp from pGE230 (p*lac*::*parA*::*gfp*) in the presence of pGE223 (p*lac*::*his6*::*parB*); (*F*) ParA-Gfp from pGE331 (*parC1* p*lac*::*parA*::*gfp*) in the presence of pGE223 (p*lac*::*his6*::*parB*); (*G*) ParA-Gfp from pGE230 (p*lac*::*parA*::*gfp*); (*H* and *I*) ParA-Gfp from pGE236G10V (*par2* Δ*parA* p*lac*::*parA*(*G10V*)::*gfp*) and pGE236K14Q (*par2* Δ*parA* p*lac*::*parA*(*K14Q*)::*gfp*), respectively; (*J*) ParA-Gfp from pGE236 (*par2* Δ*parA* p*lac*::*parA*::*gfp*) in the minicell-producing strain M2141. DAPI staining was also included (*Left*). (*K*) DAPI and Gfp signals from cells of KG22 carrying pGE236 (*par2* Δ*parA* p*lac*::*parA*::*gfp*); (*L* and *M*) DAPI staining of KG22/pGE230 (p*lac*::*parA*::*gfp*) and KG22/pGE30K (p*lac*::*lacZ′*::*gfp*) cells treated with cephalexin (10 μg/ml) and chloramphenicol (300 μg/ml). (*L′* and *M′*) Gfp signal from the same cells. Omission of chloramphenicol yielded essentially similar although less clear patterns of nucleoid distribution. (Bar = 2 μm.)

indicating that ParA-Gfp preferentially locates at nucleoid regions. This subcellular compartmentalization required neither ParB nor *parC* DNA. We did not observe oscillation in filaments, even in the presence of ParB and *parC* (not shown). By contrast, LacZ′-Gfp was evenly distributed within cells (Fig. 2 *M* and *M′*).

Discussion

Two *par* Loci. We show here that the virulence plasmid pB171 encodes two adjacent active partitioning loci, denoted *par1* and *par2* (Fig. 1*A*). Each can mediate efficient plasmid segregation alone, but optimal segregation requires the presence of both loci. Incompatibility data suggest that the two loci share a common cis-acting central site, *parC1*.

Separately, *par1* and *par2* yielded 15- and 140-fold of stabilization, respectively (Fig. 1*B*). Together, they yielded 180-fold of stabilization. Thus, the combined effect of *par1* and *par2* was less than expected from stochastically independent mechanisms. This is not surprising, because the *par* systems obviously cannot solve plasmid instability problems caused by replicon catenation, failure in plasmid replication, etc. They do, however, apparently back each other up with respect to defects in proper segregation.

The genetic organization and components of the isolated *par2* locus are in most respects typical of Type Ib loci (4). First, *parA* encodes a putative ATPase that contains the deviant Walker-type ATPase motif (10). As in other Type Ib loci, ParA of *par2* is relatively small (214 amino acids) and does not contain an N-terminal DNA-binding domain (4, 11). By analogy with *par* of pTAR (31), another Type Ib locus, ParB of *par2*, would bind to *parC1*. Furthermore, our stability and incompatibility data show that *parC2* acts as a second cis-acting site of *par2* (Fig. 1*B* and Table 1). The relatedness of the repeats in *parC1* and *parC2* suggests that ParB likely also binds to *parC2*.

ParA Undergoes Multiple Oscillations Within the Nucleoid Between Each Round of Cell Division. We find that Gfp-tagged ParA colocalizes with the nucleoid and oscillates from one end of the cell to the other several times per division cycle. Because the nucleoid itself does not appear to oscillate similarly, we infer that the protein is repositioning itself within the chromosomal mass during these oscillations. Oscillation occurs with a periodicity of about 20 min over doubling times of 75–130 min, and shorter cells in the population exhibited more rapid cycling than longer cells. The oscillating behavior of ParA was abolished in the absence of either ParB or *parC* and by a mutation in the Walker A box ATP interaction domain. Mediation of plasmid segregation is the *raison d'être* of the *par2* locus, and all three of these genetic perturbations also eliminate plasmid segregation. Thus, it seems likely that the cyclic behavior of ParA is a fundamental factor in the mechanism of plasmid DNA segregation during cell division.

However, exactly how oscillation of ParA would contribute to segregation is unclear. One question pertains to the step(s) of segregation at which oscillation would act. Perhaps oscillation is required for normal positioning of plasmid genomes at proper subcellular positions, e.g., to locate *par2*-containing plasmids at midcell and/or to relocalize the plasmid from mid- to quarter-cell positions or to nucleoid borders. Even more intriguing questions are: (*i*) How does oscillation occur at all, and (*ii*) exactly how, mechanistically, could cyclic positional alternation of a protein within the nucleoid have an effect on plasmid segregation. A possible clue is provided by the fact that ParA is known to interact with the ParB–*parC* complex. Perhaps this interaction either triggers and/or is the target of oscillation.

Three Related Cell Cycle Proteins All Exhibit Intracellular Oscillation. Oscillation of proteins from end to end within a cell has been reported previously in two other prokaryotic systems, both of which have been implicated in chromosome segregation.

Soj of Bacillus subtilis. Soj is a ParA homologue encoded by the *B. subtilis* chromosome (12). The *soj* gene is located upstream of and adjacent to *spoOJ* that encodes the *B. subtilis* ParB homologue. Soj oscillates from pole to pole or within nucleoid regions (32, 33), depending on the presence of Spo0J. Apparently, Spo0J, but not Soj, is required for chromosome partitioning. However Soj and Spo0J were both required for *parS*-dependent plasmid stabilization in *B. subtilis*. Furthermore, when cloned into a miniF replicon, the *soj spoOJ parS* locus stabilized the plasmid significantly in *E. coli* (12). The function of Soj oscillation for the *B. subtilis* chromosome is not known, but it has been suggested to be important for developmental regulation of *B. subtilis* promoters (33) or to couple developmental transcription to cell cycle progression (32). Given the results obtained here, Soj oscillation may also be involved in plasmid segregation in *B. subtilis* and *E. coli*.

MinCDE of E. coli. In many bacteria, specification of midcell septum formation is mediated by the MinCDE system. MinC is a cell division inhibitor that, in complex with MinD, counteracts Z-ring assembly (or function) by direct contact with FtsZ (34). MinE somehow limits MinCD inhibition to the cell poles and thereby allows for Z-ring assembly at midcell (35). MinE assembles as a ring-formed structure at midcell (36). MinD cell cycle proteins also belong to the superfamily of ATPases with the deviant Walker box motif (10, 37), and MinD of *E. coli* has also been shown to oscillate. Recent experiments have shown that the E-ring oscillates in concert with MinD (38, 39). The cyclic behavior of MinD and MinE suggests that the proteins confer topological specificity by keeping the concentration of MinCD complex at midcell sufficiently low as to allow Z-ring assembly.

Relationships. ParA-Gfp oscillates normally in a *minB* strain (above), indicating that oscillation of ParA occurs independently of a functional *minCDE* system. Also, there are certain differences between the MinD/E and ParA/B systems. MinD/E oscillation is more rapid than that observed for ParA and Soj (once per 20 sec rather than once per several minutes); furthermore, MinD/E are localized to the cell poles or midcell structures rather than within the nucleoid. Nonetheless, there are similarities that could point to related underlying mechanisms in all three systems. For example, in all three systems, oscillation involves a ternary complex involving the oscillating protein (ParA/Soj/MinD), a second system-encoded protein (ParB/SpoOJ/MinE), and a "structural" component (*parC1* or *parS* DNA sites or the FtsZ ring). In this regard, it would be interesting to know whether ParB oscillates. Also, cycling time varied inversely with cell size for MinD of *E. coli* (38) as well as for ParA (above).

It is also interesting that three cell cycle proteins, MinD, Soj, and ParA, all belonging to the superfamily of ATPases with the deviant Walker-type ATPase motif, exhibit multiple oscillations during the cell division cycle. This relationship allows for the speculation that other such proteins may exert their function through a dynamic subcellular localization pattern.

We thank N. Kleckner for extensive revision of the manuscript, a referee for the suggestion that ParA-Gfp associates with nucleoids, J. Møller-Jensen for the introduction to fluorescence microscopy, T. Tobe (University of Tokyo) for the donation of pB171, and O. G. Issinger for the use of a Leica microscope. The Danish Biotechnology Program supported this work.

1. Hiraga, S. (2000) *Annu. Rev. Genet.* **34**, 21–59.
2. Gordon, G. S. & Wright, A. (2000) *Annu. Rev. Microbiol.* **54,** 681–708.
3. Møller-Jensen, J., Jensen, R. B. & Gerdes, K. (2000) *Trends Microbiol.* **8,** 313–320.
4. Gerdes, K., Møller-Jensen, J. & Bugge, J. R. (2000) *Mol. Microbiol.* **37,** 455–466.
5. Watanabe, E., Wachi, M., Yamasaki, M. & Nagai, K. (1992) *Mol. Gen. Genet.* **234,** 346–352.
6. Davis, M. A., Martin, K. A. & Austin, S. J. (1992) *Mol. Microbiol.* **6,** 1141–1147.
7. Davey, M. J. & Funnell, B. E. (1994) *J. Biol. Chem.* **269,** 29908–29913.
8. Davey, M. J. & Funnell, B. E. (1997) *J. Biol. Chem.* **272,** 15286–15292.
9. Jensen, R. B. & Gerdes, K. (1997) *J. Mol. Biol.* **269,** 505–513.
10. Koonin, E. V. (1993) *J. Mol. Biol.* **229,** 1165–1174.
11. Hayes, F. (2000) *Mol. Microbiol.* **37,** 528–541.
12. Yamaichi, Y. & Niki, H. (2000) *Proc. Natl. Acad. Sci. USA* **97,** 14656–14661.
13. Gordon, G. S., Sitnikov, D., Webb, C. D., Teleman, A., Straight, A., Losick, R., Murray, A. W. & Wright, A. (1997) *Cell* **90,** 1113–1121.
14. Niki, H. & Hiraga, S. (1997) *Cell* **90,** 951–957.
15. Erdmann, N., Petroff, T. & Funnell, B. E. (1999) *Proc. Natl. Acad. Sci. USA* **96,** 14905–14910.
16. Bork, P., Sander, C. & Valencia, A. (1992) *Proc. Natl. Acad. Sci. USA* **89,** 7290–7294.
17. Dam, M. & Gerdes, K. (1994) *J. Mol. Biol.* **236,** 1289–1298.
18. Jensen, R. B., Dam, M. & Gerdes, K. (1994) *J. Mol. Biol.* **236,** 1299–1309.
19. Breuner, A., Jensen, R. B., Dam, M., Pedersen, S. & Gerdes, K. (1996) *Mol. Microbiol.* **20,** 581–592.
20. Jensen, R. B., Lurz, R. & Gerdes, K. (1998) *Proc. Natl. Acad. Sci. USA* **95,** 8550–8555.
21. Jensen, R. B. & Gerdes, K. (1999) *EMBO J.* **18,** 4076–4084.
22. Casadaban, M. & Cohen, S. N. (1980) *J. Mol. Biol.* **138,** 179–207.
23. Stougaard, P., Molin, S. & Nordstrom, K. (1981) *Proc. Natl. Acad. Sci. USA* **78,** 6008–6012.
24. Tobe, T., Hayashi, T., Han, C. G., Schoolnik, G. K., Ohtsubo, E. & Sasakawa, C. (1999) *Infect. Immun.* **67,** 5455–5462.
25. Nielsen, A. K., Thorsted, P., Thisted, T., Wagner, E. G. & Gerdes, K. (1991) *Mol. Microbiol.* **5,** 1961–1973.
26. Clark, D. J. & Maaloe, O. (1967) *J. Mol. Biol.* **23,** 99–112.
27. Walker, J. E., Saraste, M., Runswick, M. J. & Gay, N. J. (1982) *EMBO J.* **1,** 945–951.
28. Pai, E. F., Kabsch, W., Krengel, U., Holmes, K. C., John, J. & Wittinghofer, A. (1989) *Nature (London)* **341,** 209–214.
29. Story, R. M. & Steitz, T. A. (1992) *Nature (London)* **355,** 374–376.
30. Yamauchi, M. & Baker, T. A. (1998) *EMBO J.* **17,** 5509–5518.
31. Kalnin, K., Stegalkina, S. & Yarmolinsky, M. (2000) *J. Bacteriol.* **182,** 1889–1894.
32. Marston, A. L. & Errington, J. (1999) *Mol. Cell* **4,** 673–682.
33. Quisel, J. D., Lin, D. C. & Grossman, A. D. (1999) *Mol. Cell* **4,** 665–672.
34. Hu, Z. & Lutkenhaus, J. (2000) *J. Bacteriol.* **182,** 3965–3971.
35. de Boer, P. A., Crossley, R. E. & Rothfield, L. I. (1989) *Cell* **56,** 641–649.
36. Raskin, D. M. & de Boer, P. A. (1997) *Cell* **91,** 685–694.
37. Hayashi, I., Oyama, T. & Morikawa, K. (2001) *EMBO J.* **20,** 1819–1828.
38. Fu, X., Shih, Y. L., Zhang, Y. & Rothfield, L. I. (2001) *Proc. Natl. Acad. Sci. USA* **98,** 980–985. (First Published January 23, 2001; 10.1073/pnas.031549298)
39. Hale, C. A., Meinhardt, H. & de Boer, P. A. (2001) *EMBO J.* **20,** 1563–1572.
40. Gerdes, K., Larsen, J. E. & Molin, S. (1985) *J. Bacteriol.* **161,** 292–298.